Combustion and Flame 294 (2026) 115340

Contents lists available at ScienceDirect

Combustion and Flame

journal homepage: www.sciencedirect.com/journal/combustion-and-flame

Influence of water vapor on flame propagation in CH_2F-CF_3 (R-134a)/oxygen mixtures☆

Christian Schwenzer [a,*], Robert R. Burrell [b,c], Valeri I. Babushok [b], Roman Glaznev [a], Raik Hesse [a], Heinz Pitsch [a], Joachim Beeckmann [a], Gregory T. Linteris [b]

[a] Institute for Combustion Technology, RWTH Aachen University, Aachen, Germany
[b] National Institute of Standards and Technology, Gaithersburg, MD, USA
[c] Honeybee Robotics, Los Angeles, CA, USA

ARTICLE INFO

Keywords:
Refrigerant flammability
Laminar flame speed
Next-generation refrigerants
Hydrofluorocarbons
Humidity

ABSTRACT

The first laminar flame speed measurements of the hydrofluorocarbon refrigerant CH_2F-CF_3 (R-134a) with oxygen are presented for both dry and humid conditions. Flame speeds were determined from pressure-rise measurements in a spherical combustion chamber using multi-zone data reduction models that account for radiation heat losses, and the results were compared with numerical simulations. For dry mixtures, the laminar flame speed exhibits a maximum near $\phi = 0.7$, which is significantly leaner than the peak typically observed for hydrocarbon flames. Analysis of flame structure and sensitivity coefficients shows that this behavior arises from changes in the radical pool. Lean mixtures are dominated by OH-driven oxidation chemistry, while richer mixtures lean towards fluorocarbon reaction pathways that are slightly less effective at sustaining flame propagation when the equivalence ratio is increased. The influence of water vapor was examined for oxidizer water mole fractions up to 4 %. Previous studies of halogenated refrigerant flames with F/H ratio > 1 have shown a flame speed increase with added water vapor. Unexpectedly, water vapor affects laminar flame speed only slightly for the presented conditions. Our experiments indicate a small reduction in flame speed within the measurement uncertainty, while simulations predict decreases by about 6 %. Although water addition raises the peak OH concentration by approximately 75 % at $\phi = 0.7$, the overall heat release rate decreases due to shifts in reaction pathways. In particular, enhanced OH consumption through $CF_2 + OH = CFO + HF$, together with reduced heat release from fuel decomposition and fluorocarbon oxidation reactions, leads to a minor inhibition effect. Numerical calculations at higher water vapor concentrations predict a transition to strong flame speed promotion under ultra-lean conditions, where increased OH production dominates the reaction network. These results highlight the complex role of water vapor in the combustion chemistry of hydrofluorocarbon refrigerants.

Novelty and significance statement

This study provides the first experimental flame speed measurements of R-134a/O_2 mixtures and offers new insight into the influence of water vapor on fluorinated refrigerant combustion. While water vapor is often associated with combustion promotion in halogenated hydrocarbon systems through increased OH radical production, the present work shows that water vapor has only a very weak effect on laminar flame speed in R-134a/O_2 flames, with simulations and experimental trends indicating slight inhibition rather than promotion. The results show that the additional OH formed in humid mixtures can be redirected into fluorocarbon radical pathways, particularly through reactions involving CF_2, which limit the effectiveness of OH-driven chain propagation.

These findings highlight the critical role of fluorocarbon radical chemistry in controlling flame propagation in hydrofluorocarbon refrigerants and demonstrate that increased OH concentrations do not necessarily lead to enhanced reactivity. The work provides improved mechanistic understanding of the coupling between OH and CF_2 pathways in humid R-134a flames, which is important for reliable kinetic modeling and for assessing combustion behavior of refrigerants in environments where humidity may influence flame propagation.

☆ Official contribution of NIST, not subject to copyright in the United States. Certain commercial equipment, instruments, and materials are identified in this paper to adequately specify procedure. Such identification does not imply recommendation or endorsement by the National Institute of Standards and Technology.

* Corresponding author.
E-mail address: c.schwenzer@itv.rwth-aachen.de (C. Schwenzer).

https://doi.org/10.1016/j.combustflame.2026.115340
Received 7 July 2026; Received in revised form 22 September 2026; Accepted 22 September 2026
Available online 15 October 2026
0010-2180/© 2026 The Authors. Published by Elsevier Inc. on behalf of The Combustion Institute. This is an open access article under the CC BY license (http://creativecommons.org/licenses/by/4.0/).
Open access funding enabled and organized by Projekt DEAL.

1. Introduction

The refrigerant R-134a (CH_2F-CF_3, 1,1,1,2-tetrafluoroethane) is widely used and although it is being phased down, it is increasingly used as a blend component to reduce the flammability of more reactive refrigerants [1]. Hence, understanding its reactivity is important for its safe application, and consequently, it is one of twelve refrigerants in the National Institute of Standards and Technology (NIST) kinetic model that is used to predict refrigerant combustion [2]. Unlike most of the other refrigerants in the mechanism, however, laminar flame speed data for R-134a has only been measured in blends with R-32 in normal air [3]. Data for pure R-134a has not been available for refinement of the elementary kinetic rates related to its reaction.

For fluorinated refrigerants, water vapor in the reactants widens flammability limits or makes non-flammable refrigerants become flammable when the overall system is deficient in hydrogen atoms. Linteris [1] measured the laminar flame speed of several mixtures of halogenated hydrocarbons (with varying methane addition) using dry and moist air and found promotion with added water vapor, varying with the fluorine to hydrogen atom ratio in the reactants. Kondo et al. [4–6], Yang et al. [7], and Zhai et al. [8] found that mixtures of R-1234ze(E)/air were non-flammable with dry air but flammable with moist air. Takizawa et al. [9] presented experimental flame speed data on R-1234yf and R-1234ze(E) with increasing amounts of water vapor in the air and showed a strong promotion effect. Babushok and Linteris [10] calculated the flame speed of R-1234yf and R-1234ze(E) with moist and dry air at 0.101 MPa, 333 K, as well as for R-134a in air (0.101 MPa, 298 K) and showed a promotion effect by water vapor for all refrigerants. They found that adding water to mixtures of fluorine-rich refrigerant (F/H = 2) and air can generate OH, H, and O radicals which in turn raises the reaction-zone temperature and laminar flame speed.

R-134a is considered a non-combustible refrigerant [11]. However, Reed and Rizzo [12], Dekleva et al. [13], and Lisochkin and Poznyak [14] were able to ignite R-134a/air mixtures at elevated initial temperatures T_0 and pressures p_0, and at higher levels of the oxygen volume fraction in the oxidizer, although humidity was likely not controlled. Moreover, Kondo et al. [5] were not able to ignite dry mixtures of R-134a at elevated initial temperatures (333 K), but recorded the flammability limits in humid air at the same conditions.

To obtain laminar flame speed data for R-134a, experiments were performed with R-134a and oxygen, and part of these data were reported previously by Burrell et al. [15]. Our attempts to obtain self-sustained flame propagation of R-134a under standard air conditions were unsuccessful due to its low reactivity. Pure oxygen was therefore used to increase the flame speed to a measurable range, as commonly done to obtain combustion data for weakly flammable fluorinated compounds [16].

The present work uses the raw data collected in Ref. [15] and expands upon it. Since the previous evaluation used a 2-zone model without radiation treatment, the data are reprocessed here using a validated multi-zone model with radiation correction. Additional experiments with water vapor in the oxidizer are analyzed, and the laminar flame speeds are compared with predictions from a detailed kinetic model. This work provides the first experimental laminar flame speed data for R-134a and uses reaction flux and sensitivity analyses to improve the understanding of water vapor effects in refrigerant flames. These data serve as validation targets for hydrofluorocarbon kinetic models that can subsequently be used to analyze refrigerant flammability under more practical air and humidity conditions.

2. Experimental procedure and data reduction

A constant volume combustion technique was employed, as described in previous work [15,17–19]. The 1.85 L spherical stainless-steel combustion chamber has an inner diameter of 15.24 cm and centrally located tungsten electrodes. The initial mixtures were prepared using the method of partial pressures, and reactants were R-134a (99.5 %, Honeywell) and O_2 (99.5 %).

The equivalence ratio for R-134a/O_2 mixtures was calculated following the global reaction defined by Takizawa et al. [20]:

$$CH_2F{-}CF_3 + 1.5\,O_2 = CO_2 + 2\,HF + CF_2O\,. \quad (1)$$

Thus, 1.5 moles of O_2 are required per mole of R-134a for complete combustion.

When added, deionized water was injected by a hypodermic needle via a valved septum at the top into the chamber and the quantity was verified by the water vapor partial pressure. The maximum water vapor amount was limited by the 298 K saturation pressure of 3.169 kPa. This corresponds to a maximum water volume fraction in the oxidizer of approximately 5 % depending on the equivalence ratio. After each experiment, the chamber was vented and flushed with air for several minutes with a high ventilation flow rate of 8500 L/min. Experiments were conducted at a low frequency of approximately one experiment per hour. This procedure strongly diluted the exhaust gases, therefore removing all residual fluorinated combustion products, and reduced possible adsorption of acidic products such as HF on the chamber surfaces. The mixture was ignited by a capacitive discharge, and a dynamic pressure transducer collected pressure rise data at 10 kHz. Repeatability of the pressure measurements is demonstrated in the Supplementary Material (see Fig. S1) for four R-134a/O_2 experiments. The pressure signals were smoothed using a moving average filter with a window length of 20 to 50 points. Experimental data are presented over a range of conditions that are summarized in Table 1.

Laminar flame speed was computed from pressure data using the NIST constant volume data reduction tool (CVDART) [21]. The tool employs a multi-zone model [22] to divide the flame into shells that span the unburned, burned, and flame regions. The validity of pressure rise data reduction has been examined in detail by Hegetschweiler et al. [23] for R-32/air flames, whose flame speeds are comparable to those investigated here. They demonstrated the importance of radiation treatment, stretch effect consideration at small flame radii, selection of suitable data fitting limits, and use of power-law extrapolation to obtain flame speeds at initial conditions.

Each experiment was processed considering adiabaticity (ADI) and additionally with an optically-thin model (OTM) to account for radiation heat loss. These two treatments are interpreted as limiting cases: the ADI model neglects radiation heat loss, whereas the OTM model neglects reabsorption and therefore tends to overestimate the net radiative heat loss. Applying both treatments is recommended when the exact radiation model is not known [23]. The true value is expected to lie between the ADI and OTM evaluations, and their difference is treated as part of the uncertainty associated with radiation modeling. While data reduction employing a narrow-band model would be best [24], the required data for the species of interest in HFC flames at combustion temperatures are not yet available.

Closed-vessel flame speed measurements of mildly flammable refrigerants can be affected by buoyancy which has been investigated by Takizawa et al. [3]. They found that buoyancy effects are negligible for laminar flame speeds above approximately 5 cm/s. The flame speeds

Table 1
R-134a experimental conditions. Oxidizer contains O_2 and H_2O, only.

ϕ [-]	T_0 [K]	p_0 [MPa]	$X_{H_2O,ox}$ [%]
0.6	298	0.101	0, 2.4, 4
0.7	298	0.101	0, 2.4, 4
0.8	298	0.101	0
0.9	298	0.101	0
1.0	298	0.101	0, 1.7, 2.4, 3.2
1.1	298	0.101	0
1.2	298	0.101	0

reported in the present work are around 10 cm/s, and thus well above this threshold.

A previous uncertainty analysis of the present system [17,19] indicates that the maximum uncertainty for a single point measurement of R-134a/O_2 flame speed is ±12 %, or about ±1 cm/s. This uncertainty defines an interval estimated to have a level of confidence of 95 %. The uncertainty analysis follows the NIST guidelines of Taylor and Kuyatt [25] and includes uncertainties in initial temperature and pressure, dynamic pressure rise, reactant mixture preparation, equivalence ratio, and fitting.

A single experiment provides flame speed data over a range of temperatures and pressures as the flame propagates into unburned gases that are compressed near-isentropically. For screening purposes as well as for input to fire models, however, data at laboratory ambient conditions are typically desired. In the present work, initial conditions in the chamber are ambient $T_0 = 298$ K and $p_0 = 0.101$ MPa but the early data are unusable due to flame stretch, ignition disturbances, and noise due to large scatter in the derivatives of $p(t)$ because of low pressure rise for very small flame radii. Hence, to obtain the unstretched laminar flame speed $S^0_{L,u}$ at the initial conditions (T_0, p_0), $S_{L,u}(p)$ data are fitted to a curve, e.g. power-law or Arrhenius-type, obtained at higher pressure and temperature and extrapolated to p_0, T_0 [23]. In the present work, a power-law fit was used because it has been found to be more accurate than the Arrhenius-type for R-32/air flames [23]. The power-law reads

$$S_{L,u} = S^0_{L,u} \left(\frac{p}{p_0} \right)^{\alpha} . \tag{2}$$

$S_{L,u}(p)$ is fitted to pressure only because the temperature in the compressed unburned gas is directly connected to pressure via the isentropic relationship:

$$T = T_0 \left(\frac{p}{p_0} \right)^{\frac{\gamma-1}{\gamma}} . \tag{3}$$

The near-isentropic relation is consistent with the multi-zone constant-volume formulation.

To apply the power-law fit in Eq. (2), a data range must be selected. Fig. 1 shows $p(t)$ data for three values of equivalence ratio. The pressure rise is small in the early stages because the flame radius is small relative to the chamber size. The rate of pressure rise increases as the flame radius increases until the flame starts to lose heat to the chamber walls which usually coincides with the inflection point in the pressure curve at $max\{\dot{p}\}$. As discussed previously [23], only a portion of the $p(t)$ data are used for the power-law fit. Cropping of $S_{L,u}(p)$ data at the lower end eliminates ignition disturbances as well as stretch effects, which are more important at small radii. Chen et al. [26] demonstrated that the influence of stretch on laminar flame speed is negligible when the chamber pressure exceeds 2 times the initial value. We therefore selected a lower bound of $2p_0$ for all the cases in this study. We showed the suitability of this value already for R-32/air flames with similar flame speed and composition to the present flames in our previous study [23].

The upper end of $S_{L,u}(p)$ data eliminates effects from flame instabilities and wall heat loss. In Fig. 1, the inflection point is indicated by the black triangles, and the symbols (•, –, and –) indicate values of 40, 60, and 80 % of the inflection point pressure for that curve, respectively. Depending on the fuel, mixture, and conditions, cellular flame instabilities can cause flame acceleration and an increase in slope prior to the advent of wall effect, for example those discussed by Moghaddas et al. [27] for R-152a/air flames. To avoid fitting to unstable $S_{L,u}$ data, we apply our approach presented by Bariki et al. [28] which analyzes the pressure signal to identify the onset of instabilities. In this way, an upper cropping limit at the appearance of the first instance of flame acceleration is selected.

In Fig. 1, the section of data used in the power law fit is indicated by the thick portion of each curve. More details on the fit range selection and sensitivity of the extrapolated $S^0_{L,u}$ are given in the supplementary material.

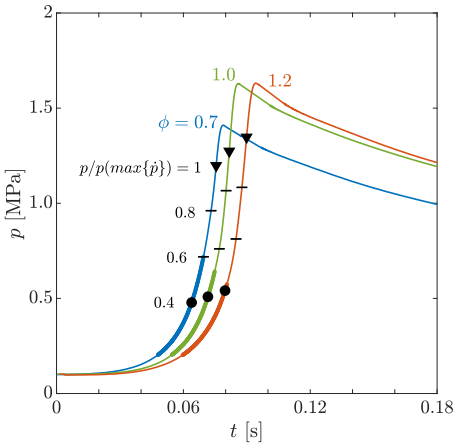


Fig. 1. Experimentally measured dynamic pressure in the chamber (solid lines) as a function of time for R-134a/O_2 mixtures for the indicated value of ϕ. The data used for fitting are indicated by the thick lines. The curves are marked at specific fractions of p of the inflection point: 0.4, 0.6, 0.8, 1.0, given by the symbols •, –, –, and ▼, on each curve, respectively.

3. Numerical framework

Flame speed simulations for planar, stationary flames are performed using the appropriate modules in FlameMaster [29] as well as Cantera [30]. The equations of mass, species, and energy conservation are solved numerically. Simulations are conducted for adiabatic (ADI) flames (no radiation) and for flames computed with an Optically Thin Model (OTM) for radiation. In FlameMaster, the global reaction (see Eq. (1)) was explicitly defined to compute the equivalence ratio. For Cantera calculations, the mole fractions were calculated beforehand and used to define the unburned mixture. Reaction mechanism analysis is performed with the graphical post-processing Xsenkplot [31] as well as in-house MATLAB routines. The kinetic model is that developed previously by Babushok et al. [2] for predicting the flame speed of hydrofluorocarbon (HFC) refrigerants (R-32, R-41, R-125, R-134, R-134a, R-143, R-152, R-152a, R-227ea, R-1234yf, and R-1234ze(E)) and their blends in air for which experimental data were available in the literature (typically for ambient conditions with data reduction performed with a two-zone model and neglecting thermal radiation heat losses). The mechanism has 1064 reactions with 113 species and was developed based on earlier work [32–34].

4. Results and discussion

4.1. Flames in dry air

Fig. 2 shows the measured flame speed of the R-134a/O_2 flames as a function of pressure in the spherical combustion chamber for three values of equivalence ratio ϕ. Thin solid lines show the experimental data, the thick portions of these lines mark the data used for the curve fit, and the dotted lines show the power-law curve fit. The triangles at $p = 0.101$ MPa show the extrapolated values of $S_{L,u}$ at T_0, p_0 using the power-law. Other symbols in the figure (•, –, –, and ▼) denote 0.4, 0.6, 0.8, and 1.0 of the inflection point pressure as in Fig. 1.

The lean flames ($\phi = 0.7$) have the highest values of $S_{L,u}$, while those of stoichiometric and rich are lower. As time progresses and unburned gas temperature and pressure increase, all three curves show flame acceleration at pressure values below the inflection point. At pressures slightly higher than p_0, the experimental data are subject to large scatter due to the influence of the ignition and the pressure measurement uncertainty far below the full-scale value of the pressure transducer. At later times, the ignition energy has decayed and the

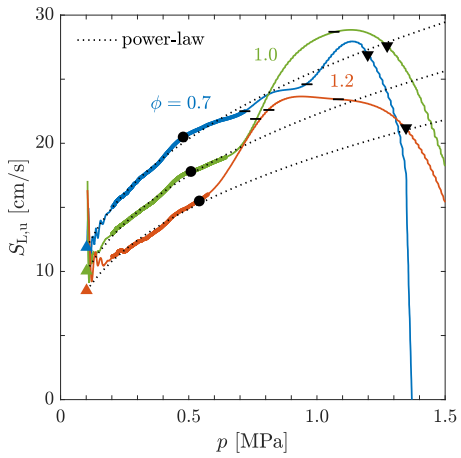


Fig. 2. Experimental $S_{L,u}$ calculated from the measured pressure rise as a function of the unburned gas pressure (Initial conditions: 298 K, 0.101 MPa). Data are radiation-corrected using OTM. The curves are marked at specific fractions of p of the inflection point: 0.4, 0.6, 0.8, 1.0, given by the symbols •, –, –, and ▼, on each curve, respectively.

influence of stretch diminishes due to the larger flame radius and higher pressure.

The importance of radiation heat losses to the propagation of near-limit, outwardly propagating spherical flames has been discussed in previous works [24,35–40]. To illustrate the importance of the data reduction radiation model on the inferred value of the flame speed, Fig. 3 shows the extrapolated value of $S^0_{L,u}$ for dry R-134a/O_2 flames from the present data reduction using the 2-zone model, which is adiabatic, together with results using the multi-zone ADI model and the multi-zone model employing OTM for radiation-correction. The 2-zone model and the multi-zone ADI model yield nearly identical $S^0_{L,u}$ values while the multi-zone OTM model is about 7.6 % higher than the ADI models.

While it may seem counterintuitive that the OTM data is higher than the ADI data, the label refers to the correction for radiation effects used in the data reduction as has been previously discussed [23]. Radiative heat losses from the burned gases reduce the measured pressure rise and therefore lead to lower apparent flame speeds if they are neglected.

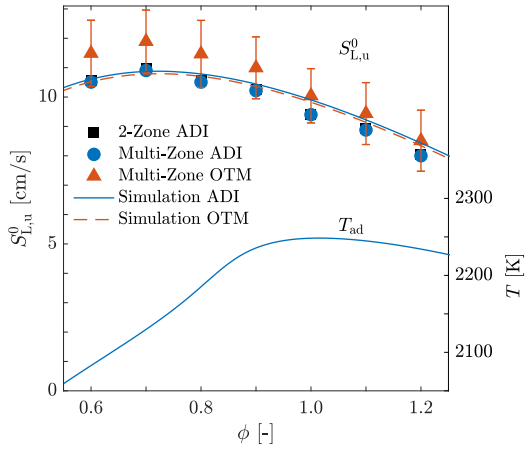


Fig. 3. Laminar flame speed and adiabatic flame temperature versus equivalence ratio at 298 K, 0.101 MPa. Symbols represent experimental laminar flame speed values of dry R-134a/O_2 mixtures for data reduction employing the 2-zone ADI, Multi-zone ADI, and Multi-zone OTM models. Lines represent numerical predictions (steady, planar) for ADI and OTM configurations.

Correcting for this effect increases the inferred flame speed, which explains why the OTM-corrected values are higher than the ADI results.

Laminar flame speed predictions with ADI and OTM radiation assumptions are shown by the solid and dashed lines, respectively. The numerical predictions for ADI and OTM are very close because they exclusively depict the effect of radiation on chemistry. In the experiment, flames are also subject to a kinematic deceleration effect caused by the inward motion of cooling burned gas as has been observed for other refrigerant flames [41,42]. In the development of the kinetic model, some of the elementary rate expressions were adjusted within their uncertainty to match the numerically calculated adiabatic flame speed with literature experimental values, obtained exclusively from pressure rise experiments without consideration of radiation in the data reduction (i.e., using a 2-zone, adiabatic model).

For all data reduction models and numerical predictions shown in Fig. 3, the maximum value of $S^0_{L,u}$ occurs near $\phi = 0.7$, which is significantly leaner than the peak typically observed for hydrocarbon flames. In addition, the decrease in reactivity away from this maximum is less pronounced than in hydrocarbon systems, a behavior previously reported for other halogenated hydrocarbon flames [34,43]. The computed adiabatic flame temperature plotted on the secondary y-axis reaches its maximum close to stoichiometry and does not coincide with the laminar flame speed trends. This observation suggests that the controlling chemistry differs from classical hydrocarbon oxidation due to the unique nature of fluorocarbon pathways. To understand the origin of this behavior, the flame structure, radical pool composition, and sensitivity of the flame speed to key reactions are analyzed.

Fig. 4 shows flame profiles of key species mole fractions X_i, together with the local temperature T and heat release rate $\dot{q}$ for adiabatic flames. The zero-value is located at the peak of the heat release rate $\dot{q}$. At stoichiometric conditions, $\dot{q}$ reaches its maximum with respect to equivalence ratio and is only slightly lower at $\phi = 0.7$, while it decreases substantially at $\phi = 1.2$. At the same time, the temperature at the location of peak heat release is lowest for $\phi = 0.7$. This suggests that the peak in laminar flame speed is not governed solely by temperature or global heat release, but rather by changes in the radical pool and the dominant reaction pathways as the equivalence ratio varies.

The mole fraction profiles of OH (scaled by a factor of 100), CF_2, and CF_3 reveal a significant restructuring of the radical pool with equivalence ratio. The peak mole fractions of CF_2 and OH exhibit nearly mirrored behavior: CF_2 concentrations increase towards richer mixtures while OH concentrations decrease, with intermediate values at stoichiometric conditions. The CF_3 mole fraction increases from lean to stoichiometric mixtures and then approaches a plateau at richer conditions.

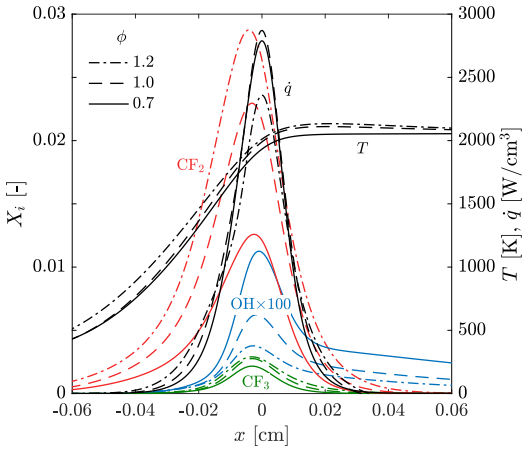


Fig. 4. Flame structure of R-134a/O_2 mixture at initial conditions: p_0 = 0.101 MPa, T_0 = 298 K for varying equivalence ratios.

The sensitivity analysis shown in Fig. 5 indicates that the laminar flame speed is most sensitive to reactions involving these species and that their relative importance depends on equivalence ratio. It should be noted that the normalized sensitivity coefficients describe the response of $S^0_{L,u}$ to individual rate constants, whereas the overall role of a pathway depends on the absolute reaction flux through that pathway.

Under lean conditions, hydrocarbon-like oxidation chemistry becomes more influential. The reaction OH+CO = H+CO_2, which strongly promotes flame propagation, exhibits its highest positive sensitivity near $\phi = 0.7$. This is consistent with the elevated OH concentrations observed in the lean flame. As the mixture becomes richer, fluorocarbon chemistry becomes more important due to the increased availability of CF_2 and CF_3. Although several normalized sensitivity coefficients associated with fluorocarbon reactions slightly decrease in magnitude at richer conditions, the absolute flux through many fluorocarbon pathways increases due to the higher concentrations of these intermediates. Flame-speed-promoting oxidation reactions such as $CF_2 + O_2 = CF_2O + O$ and $CF_3 + O_2 = CF_3O + O$ become more relevant and reactions of the fuel decomposition products involving CHF−CF_2 and CHF−CF_3 contribute more to flame speed reduction. These reactions generate additional CF_2 and CF_3 radicals and shift the chemistry towards slower fluorocarbon pathways.

A key link between the hydrocarbon and fluorocarbon pathways is the reaction $CF_2 + OH = CFO + HF$, which couples CF_2 and OH chemistry and removes reactive radicals from the system. As the equivalence ratio increases and CF_2 concentrations rise, this pathway becomes more active and reduces the availability of OH for flame-speed-promoting reactions. The OH mole fraction depends on the availability of oxygen and is therefore strongly limited under richer conditions, whereas CF_2 and CF_3 originate solely from the fuel and therefore always increase with ϕ. Consequently, the balance between OH-driven oxidation chemistry and CF_x radical chemistry governs the dependence of laminar flame speed on equivalence ratio. Under lean conditions, the higher OH concentration favors reactions that accelerate flame propagation, whereas at richer conditions the increasing importance of CF_x chemistry and associated radical-consuming pathways reduces the overall reactivity.

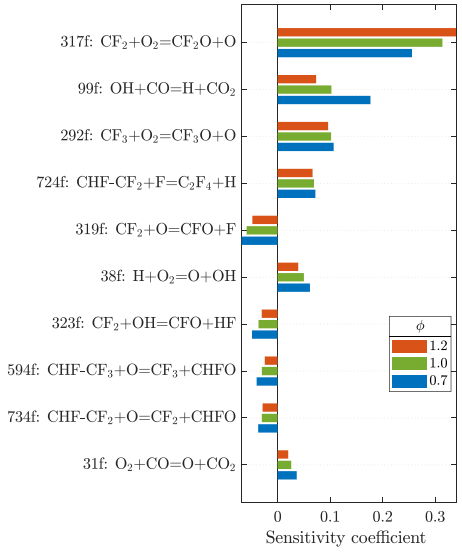


Fig. 5. Normalized sensitivity coefficients for $S^0_{L,u}$ with respect to frequency factors of rate coefficients for R-134a/O_2 flames. The initial conditions vary in equivalence ratio at constant pressure and temperature of 0.101 MPa and 298 K.

4.2. Flames with water vapor

The effect of water vapor on the laminar flame speed is shown in Fig. 6, where experimental measurements and numerical predictions are compared for mixtures containing up to 4 % H_2O in the oxidizer stream. Unexpectedly, water vapor affects laminar flame speed only slightly. The experimental data indicate a decrease in $S^0_{L,u}$ with added water vapor, although the magnitude of this change remains within the combined measurement uncertainty. Therefore, the experiments do not establish a statistically unambiguous inhibition effect. Numerical simulations predict a similar trend, with reductions in laminar flame speed of about 6 %. The deviation between experiments and simulations at lean conditions is largest and almost outside the measurement uncertainty. Considering the additional uncertainty associated with the overestimation of radiation heat loss by OTM, the lean experimental data are still consistent with the numerical predictions. The weak response to water vapor contrasts with other humid hydrofluorocarbon and hydrofluorolefin flames, where water vapor commonly produces strong laminar flame speed promotion [10].

The computed adiabatic flame temperature, plotted on the secondary y-axis of Fig. 6, changes by less than 8 K with water vapor addition and its maximum remains at stoichiometry. This emphasizes the decoupled nature of laminar flame speed and adiabatic flame temperature. To separate dilution and chemical effects, an additional simulation was performed at $\phi = 0.7$ in which the 4 % water vapor in the reactant mixture was replaced by an artificial inert species with the thermodynamic properties of water. The dry flame has $T_{ad} = 2130$ K and $S^0_{L,u} = 10.87$ cm/s. Adding normal chemically active water increases the adiabatic flame temperature slightly to $T_{ad} = 2138$ K, but decreases the laminar flame speed to $S^0_{L,u} = 10.17$ cm/s. The inert water case gives the same adiabatic flame temperature, $T_{ad} = 2138$ K, but a higher flame speed of $S^0_{L,u} = 10.38$ cm/s. Thus, the slight decrease in $S^0_{L,u}$ is only partially caused by dilution, while the additional reduction observed with water is caused by changes in the reaction chemistry. To unravel the minor water vapor effect, the following analysis looks at changes in flame structure, radical pool composition, and the influence of water on the initial fuel decomposition reactions and associated heat release.

The flame structure for dry and humid mixtures at $\phi = 0.7$ is shown in Fig. 7. Mole fractions of OH, CF_2, and CF_3 all peak within the main reaction zone. Adding 4 % water vapor increases the peak OH mole fraction by approximately 75 % whereas the peak CF_2 mole fraction decreases by 30 % and remains largely insensitive to variations

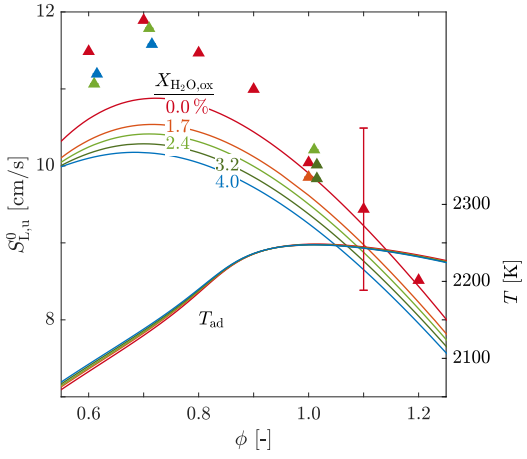


Fig. 6. Laminar flame speed and adiabatic flame temperature versus equivalence ratio at 298 K, 0.101 MPa with and without added water vapor. Symbols represent experimental laminar flame speed values of dry R-134a/O_2 mixtures for data reduction employing the Multi-Zone OTM model. Lines represent ADI numerical predictions (steady, planar).

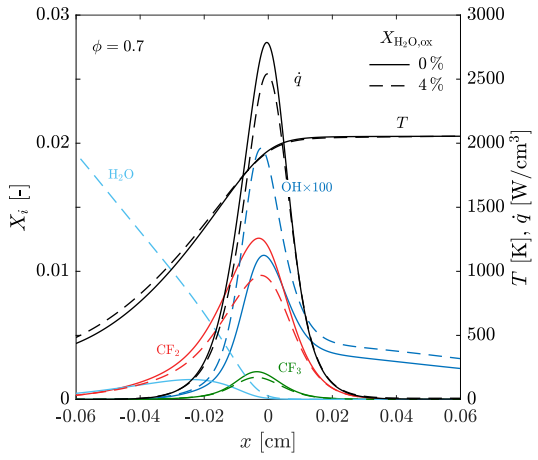


Fig. 7. Flame structure of R-134a/O_2 mixture at initial conditions: $\phi = 0.7$, $p_0 = 0.101$ MPa, $T_0 = 298$ K. Dry and wet (4 % H_2O in the oxidizer) reactant mixtures are shown as solid and dashed lines, respectively.

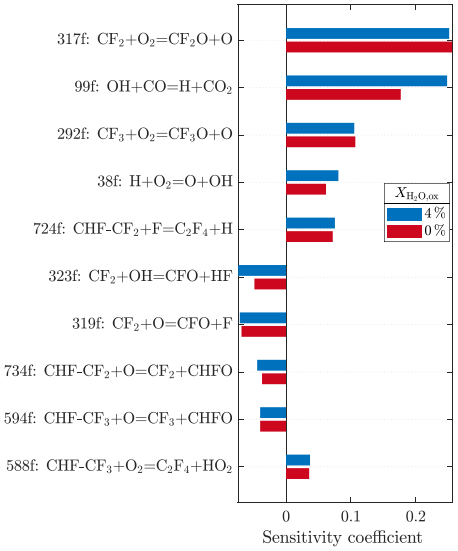


Fig. 8. Normalized sensitivity coefficients for $S^0_{L,u}$ with respect to frequency factors of rate coefficients for CH_2F-CF_3 (R-134a)/O_2/H_2O flames. The initial conditions vary in water vapor mole fractions at constant pressure, temperature, and equivalence ratio of 0.101 MPa, 298 K, and $\phi = 0.7$.

in rate constants, indicating that its concentration is controlled by quasi-equilibrium within the reaction zone.

In many halogenated hydrocarbon flames with global F/H ratio > 1, the addition of water vapor would typically promote flame propagation through the reaction

$$H_2O + F = OH + HF,$$

which converts F radicals into OH radicals [10,44]. Although the mixture approaches saturation at $X_{H_2O,ox} = 4.58\,\%$ for $\phi = 0.7$, the absolute amount of water remains small compared to the fuel and oxygen because the mixture contains no inert diluent such as N_2. Consequently, the classical H_2O-promotion pathways are activated but do not dominate the reaction network.

In the present system, the peak heat release decreases by about 8 %, closely matching the reduction in laminar flame speed. The temperature profiles of the dry and wet flames are nearly identical, except for a slightly earlier temperature rise in the preheat region of the wet flame, which increases the thermal flame thickness by approximately 9 %.

Sensitivity coefficients shown in Fig. 8 show that most reactions governing the laminar flame speed are only weakly affected by water addition. Two reactions play an exceptionally important role: the flame-speed–promoting reaction $OH + CO = H + CO_2$ and the reaction $CF_2 + OH = CFO + HF$, which becomes a stronger sink for OH radicals in the wet flame. The latter reaction removes both OH and the fluorocarbon species CF_2, thereby acting as a chain-terminating pathway that limits the effective radical pool sustaining flame propagation.

The balance of OH formation and consumption in the reaction zone is summarized in Table 2. The values correspond to rates integrated over one flame thickness around the peak temperature gradient. Details of the localized production of OH are provided in the supplementary Figure S6.

With water addition the total OH formed and consumed increases substantially because the reaction $H_2O + F = OH + HF$ becomes a major OH formation pathway. In contrast, the absolute rate of the classical chain-branching reaction $H + O_2 = O + OH$ remains nearly unchanged, reducing its relative contribution to OH formation. Although the distribution of OH consumption pathways changes only slightly, the increased OH concentration leads to a higher reaction flux through $CF_2 + OH = CFO + HF$. The OH-consuming pathways involving the fuel radicals $CHF-CF_2$ and $CHF-CF_3$ are increased. Consequently, a significant fraction of the additional OH radicals produced from water is rapidly consumed through fluorocarbon pathways rather than contributing to chain-branching reactions.

Table 2
OH formation and consumption reactions sorted by amount formed/consumed in the reaction zone of a dry flame and a wet flame with 4 % water vapor in the oxidizer. Detailed production rates are shown in the supplementary material Figures S6 (a) and (b).

Reaction	OH converted in reaction zone [mol/m^3/s] dry	wet
formation:		
$H + O_2 = O + OH$	0.367	0.386
$H_2O + F = OH + HF$	0.181	0.441
$CH_2F-CF_3 + O = CHF-CF_3 + OH$	0.082	0.072
$CHF-CF_3 + HO_2 = CF_3 + CHFO + OH$	0.048	0.047
$CF_2 + HO_2 = CF_2O + OH$	0.036	0.031
$CHFO + O = CFO + OH$	0.033	0.031
total amount formed	0.831	1.098
consumption:		
$OH + CO = H + CO_2$	−0.182	−0.252
$CF_2 + OH = CFO + HF$	−0.164	−0.195
$CH_2F-CF_3 + OH = CHF-CF_3 + H_2O$	−0.162	−0.229
$OH + F = O + HF$	−0.118	−0.138
$CHF-CF_3 + OH = CHO-CF_3 + HF$	−0.089	−0.115
$CHF-CF_2 + OH = CHFO + CHF_2$	−0.024	−0.039
total amount consumed	−0.828	−1.096

Water addition further modifies the initial fuel decomposition pathways, as illustrated in Fig. 9. The decomposition of R-134a proceeds through both thermal decomposition and radical attack. With water present, the balance of radical attack shifts slightly from F-atom reactions towards thermal decomposition and OH-initiated reactions. Because F-atom attack pathways contribute significantly to the heat release during the early stages of fuel conversion, this shift reduces the heat released during the fuel breakup process. Further down in the fuel break-up process, similar observations can be made. $CHF-CF_3 + CF_3$ pathways are almost halved in the humid flames while $CHF-CF_3 + OH$ increases by 50 %. Reactions of $CHF-CF_2$ with F are lessened and the oxidation pathway via O radicals slightly grows to produce most of the smaller fluorocarbon species.

The impact of these pathway changes on the heat release is illustrated in Fig. 10, which compares the total net heat release rate with contributions from different groups of reactions.

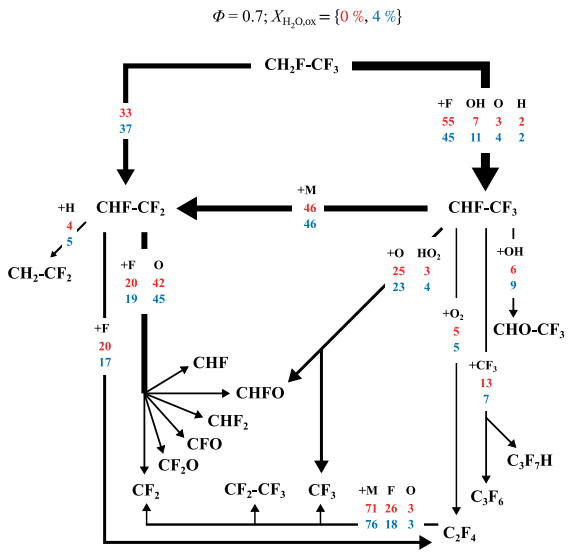


Fig. 9. Dominant reaction pathways for decomposition of R-134a at initial conditions of 0.101 MPa, 298 K, $\phi = 0.7$, and varying $X_{H_2O,ox}$. Each arrow connects a reactant and product of interest; for each reaction route, the reaction partner and the percentage of the reactant that goes through that route are indicated.

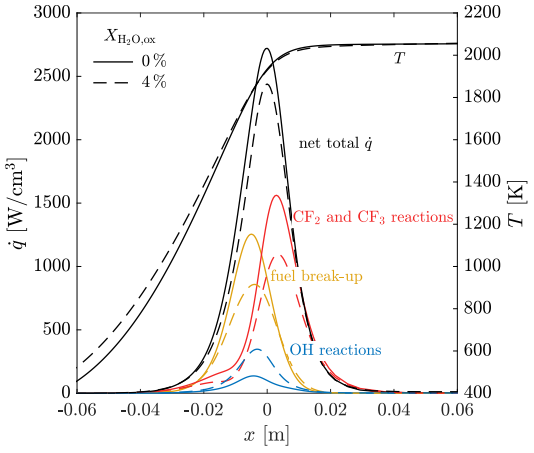


Fig. 10. Net heat release rates and temperature at 0.101 MPa, 298 K, $\phi = 0.7$, and varying $X_{H_2O,ox}$. Bell-shaped curves correspond to specific sums of heat release rates.

Each curve, except the net total, corresponds to a unique set of reactions to avoid double counting of heat release contributions. The yellow curve plots the release rate from reactions involving the top three species shown in Fig. 9 which are the fuel (R-134a) and the two fuel decomposition products (CHF−CF_2 and CHF−CF_3). The red curve represents the heat release of CF_2 and CF_3 reactions excluding those of the fuel and fuel decomposition products. Finally, the blue curve corresponds to the heat release from OH reactions excluding reactions with the fuel, fuel decomposition products, CF_2, and CF_3. A detailed breakdown of the individual heat release rates for the dominant reactions is provided in the supplementary material (see Fig. S7).

The comparison shows that the contributions associated with fuel decomposition decrease noticeably in the humid flame. This reduction reflects the shift in the initial fuel conversion pathways discussed above, where radical attack moves partially from F-atom reactions towards OH-initiated reactions with water added to the reactants. Because F-atom attack pathways are strongly exothermic during the early stages of fuel oxidation, their reduced importance lowers the heat released during fuel breakup.

In addition, the oxidation of fluorocarbon radicals contributes less heat release when water is present. Several reactions involving CF_x species, such as

$$CF_2 + O_2 = CF_2O + O,$$
$$CF_2 + O = CFO + F,$$
$$CF_3 + O = CF_2O + F$$

are less active in the wet flame. These reactions represent important exothermic oxidation pathways in the dry flame and contribute significantly to the overall heat release within the main reaction zone. Their reduced activity therefore leads to a further decrease in the total heat release rate. At the same time, reactions involving OH become more active due to the increased OH radical pool generated through $H_2O + F = OH + HF$. While these reactions locally enhance reactivity and contribute to additional heat release, their overall contribution is insufficient to compensate for the reduced energy release associated with the consumption of the fuel and highly reactive fluorocarbon fragments. Consequently, the combined effect of these pathway shifts is a lower total heat release rate in the humid flame, which is consistent with the slight reduction in laminar flame speed.

4.3. Effects at higher water vapor concentrations

So far, inhibition effects in R-134a/O_2 flames have been analyzed at low water vapor concentrations, but interesting phenomena emerge when humidity levels are significantly higher. At 298 K and 0.101 MPa, water mole fractions above 3.169 % (3.4 % $\leq X_{H_2O,ox} \leq$ 6.2 % for $0.1 \leq \phi \leq 1.5$) exceed the saturation limit, yet investigating elevated water contents provides valuable insights into flame propagation because they are more comparable to refrigerants that have higher stoichiometric oxygen coefficients such as R-1234yf. For R-1234yf, 4 % water in the oxidizer corresponds to 1.7 times more water relative to the fuel than in the R-134a mixtures. Similarly, the ratio between water and fuel is five times higher when normal air is used instead of pure oxygen.

To explore these effects, higher water vapor concentrations were examined via numerical calculations. Here, the behavior changes significantly and numerical simulations predict strong flame speed promotion under certain conditions. This underlines that the influence of water depends on the balance between competing reaction pathways and can shift as the radical pool changes with humidity and equivalence ratio. The evolution of laminar flame speed and changes in the OH radical pool and the corresponding temperature are examined over a wide range of equivalence ratios and water concentrations to clarify this transition.

Fig. 11 (top frame) shows laminar flame speed predictions for equivalence ratios in the range $0.1 \leq \phi \leq 1.5$ and water vapor mole fraction $X_{H_2O,ox}$ from 0 % to 20 %. Substantially lower ϕ values are included to capture the pronounced flame speed enhancement observed under ultra-lean conditions ($\phi < 0.6$) . The promotion effect with added water vapor on the ultra-lean side is striking, with a distinct flame speed peak forming. For mildly rich flames, there is always inhibition while for $0.5 < \phi < 1.0$, the behavior switches depending on $X_{H_2O,ox}$ and ϕ. At $X_{H_2O,ox} = 4$ %, flames with $\phi = 0.3$ and $\phi = 0.7$ yield nearly the same flame speed. Increasing the humidity further enhances this lean flame speed peak and shifts it slightly towards richer mixtures.

Fig. 11 (bottom frame) plots the maximum OH mole fraction and the corresponding temperature at that location for super-saturated R-134a/O_2/H_2O flames. As indicated, the OH radical pool dominates in the lean region with increasing water vapor content. The flame zone temperature remains relatively unchanged at low humidity levels but eventually scales with the peak OH mole fraction. The water content must exceed an initial threshold in lean R-134a flames until the additional OH production controls the flame speed. On the rich side,

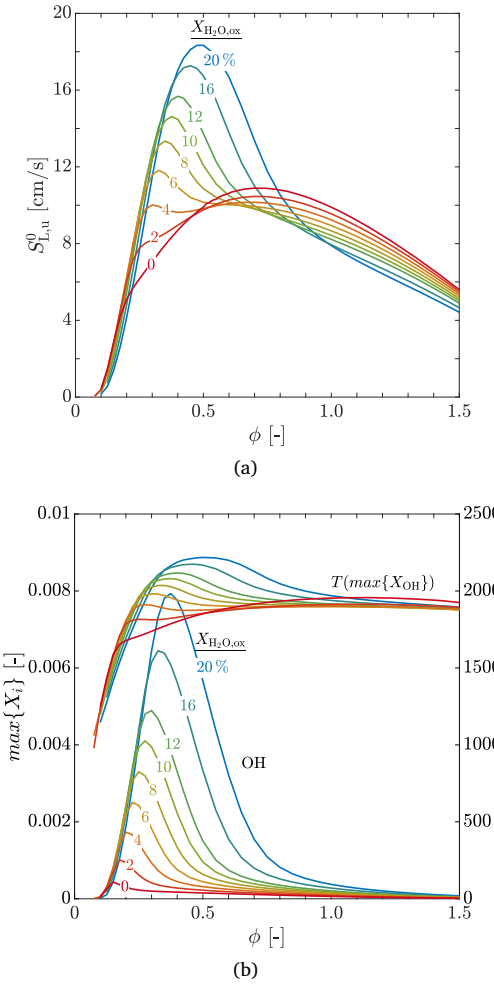


Fig. 11. Numerical predictions of R-134a/O_2 mixtures (initial conditions: 298 K, 0.101 MPa) with increasing molar fractions of water vapor in the oxidizer. Laminar flame speed over equivalence ratio (top) and peak OH mole fraction and corresponding temperature over equivalence ratio (bottom).

OH levels only increase slightly because of the additional consumption with CF_2.

Fig. 12 traces the peak laminar flame speed across different water concentrations. The peak flames speed decreases before shifting to the promotion region. As mentioned before, the inhibitory effects at low water contents ($0 < X_{H_2O,ox} < 4\,\%$) predicted for equivalence ratios above $\phi = 0.6$ are comparatively subtle and therefore difficult to confirm experimentally given that the uncertainties exceed the magnitude of the inhibition itself. Future investigations focusing on mixtures with higher water content, particularly at ultra-lean conditions, could provide additional information on the mechanism of humidity influence on the combustion of hydrofluorocarbon refrigerants.

5. Conclusions

Experiments were performed in a spherical combustion chamber at 298 K and 0.101 MPa to obtain the first laminar flame speed measurements of R-134a/O_2 mixtures. The results were compared with numerical simulations to investigate the influence of equivalence ratio and water vapor on flame propagation. Overall, the simulations reproduce the experimental trends and provide useful insight into the governing reaction pathways.

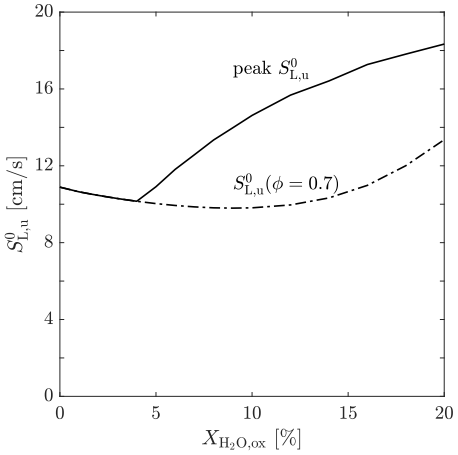


Fig. 12. Extracted peak $S^0_{L,u}$ plotted over $X_{H_2O,ox}$ for initial conditions: p_0 = 0.101 MPa, T_0 = 298 K.

For dry mixtures, the laminar flame speed exhibits a maximum near $\phi = 0.7$, which is significantly leaner than the peak typically observed for hydrocarbon–air flames and other hydrofluorocarbon-air flames. In addition, the decrease in flame speed away from this maximum is less pronounced than in hydrocarbon systems. Computed adiabatic flame temperature peak near stoichiometry highlighting the decoupled nature of laminar flame speed and adiabatic flame temperature in hydrofluorocarbon flames. Analysis of flame structure and sensitivity coefficients shows that the dependence of laminar flame speed on equivalence ratio is not governed primarily by temperature or global heat release, but by changes in the radical pool and the dominant reaction pathways. Lean mixtures exhibit higher OH concentrations and stronger hydrocarbon-like oxidation chemistry, particularly through the flame-speed–promoting reaction OH + CO = H + CO_2. As the mixture becomes richer, the chemistry shifts towards fluorocarbon pathways characterized by increased formation and consumption of CF_2. Because these fluorocarbon reaction pathways are generally less effective at sustaining chain propagation than the OH-driven oxidation chemistry, this shift leads to a gradual reduction in laminar flame speed with increasing equivalence ratio despite higher flame temperatures.

The addition of small amounts of water vapor (1.7–4 % in the oxidizer) unexpectedly have almost no effect on laminar flame speed. Experiments indicate a slight decrease in laminar flame speed within the measurement uncertainty, while simulations predict reductions of up to approximately 6 %. Although the addition of water substantially increases the OH radical concentration by about 75 % at $\phi = 0.7$, this does not enhance flame propagation. Instead, the peak heat release rate decreases and the thermal flame thickness grows slightly. Reaction pathway analysis shows that water alters the dominant OH formation routes by introducing the reaction $H_2O + F = OH + HF$ as a major OH source. However, the additional OH is largely consumed through fluorocarbon pathways rather than contributing to chain propagation. In particular, the reaction $CF_2 + OH = CFO + HF$ acts as an effective chain-terminating pathway and competes with the flame-speed–promoting reaction OH + CO = H + CO_2. At the same time, water shifts the initial fuel decomposition chemistry from exothermic F-atom attack towards OH-initiated pathways and reduces the activity of several exothermic CF_x oxidation reactions. The combined effect of these changes is a modest reduction in the overall heat release, which explains the slight inhibition of laminar flame speed observed in humid R-134a/O_2 flames.

Numerical calculations performed for higher water vapor concentrations reveal that the influence of water depends strongly on equivalence ratio. At moderate humidity levels, the minor inhibition observed experimentally persists for $\phi \gtrsim 0.6$. However, at substantially higher

water concentrations, a pronounced promotion effect appears under ultra-lean conditions. In this regime, increasing water vapor significantly enhances the OH radical pool and leads to the formation of a new flame speed maximum at very lean equivalence ratios. Future experiments at elevated initial temperature can test this transition directly, since higher temperatures allow larger water vapor mole fractions in the mixture.

CRediT authorship contribution statement

Christian Schwenzer: Writing – original draft, Visualization, Validation, Methodology, Investigation, Formal analysis, Data curation, Conceptualization. **Robert R. Burrell:** Validation, Methodology, Investigation, Formal analysis. **Valeri I. Babushok:** Writing – review & editing, Writing – original draft, Validation, Methodology, Investigation, Data curation, Conceptualization. **Roman Glaznev:** Writing – review & editing, Investigation. **Raik Hesse:** Writing – review & editing, Investigation. **Heinz Pitsch:** Writing – review & editing, Validation, Supervision, Software, Methodology. **Joachim Beeckmann:** Writing – review & editing, Validation, Supervision, Resources, Project administration, Methodology, Funding acquisition, Conceptualization. **Gregory T. Linteris:** Writing – review & editing, Writing – original draft, Visualization, Validation, Supervision, Software, Resources, Project administration, Methodology, Investigation, Funding acquisition, Conceptualization.

Declaration of competing interest

The authors declare that they have no known competing financial interests or personal relationships that could have appeared to influence the work reported in this paper.

Acknowledgments

The work at NIST was supported by the U.S. Department of Defense, Strategic Environmental Research and Development Program (SERDP), project WP19-1385, and the U.S. Office of Naval Research (Project Manager Mark Spector) under MIPR N0001422IP00032. Christian Schwenzer, Roman Glaznev, Raik Hesse, Joachim Beeckmann, and Heinz Pitsch acknowledge the funding by the Deutsche Forschungsgemeinschaft (DFG, German Research Foundation) under Research Unit FOR 5507 with project number 497007546. Computing time provided at the RWTH Aachen University (project number rwth1433) is gratefully acknowledged.

Appendix A. Supplementary material

Supplementary material related to this article can be found online at https://doi.org/10.1016/j.combustflame.2026.115340.

References

[1] G.T. Linteris, Test Results Prepared for DuPont Explosion Hazard Lab: Burning Velocity Tests of Halocarbons in Air, NIST Tech. N., 1999.
[2] V.I. Babushok, D.R. Burgess Jr., D.K. Kim, M.J. Hegetschweiler, G.T. Linteris, Modeling of Combustion of Fluorine-Containing Refrigerants, NIST Tech. N., 2021.
[3] K. Takizawa, S. Takagi, K. Tokuhashi, S. Kondo, M. Mamiya, H. Nagai, Assessment of burning velocity test methods for mildly flammable refrigerants, part 1: Closed-vessel method, ASHRAE Tran. 119 (2013) 243.
[4] S. Kondo, K. Takizawa, A. Takahashi, K. Tokuhashi, J. Mizukado, A. Sekiya, Flammability limits of olefinic and saturated fluoro-compounds, J. Hazard. Mater. 171 (2009) 613–618.
[5] S. Kondo, K. Takizawa, K. Tokuhashi, Effects of temperature and humidity on the flammability limits of several 2L refrigerants, J. Fluor. Chem. 144 (2012) 130–136.
[6] S. Kondo, K. Takizawa, K. Tokuhashi, Effect of high humidity on flammability property of a few non-flammable refrigerants, J. Fluor. Chem. 161 (2014) 29–33.
[7] Z. Yang, X. Wu, T. Tian, Flammability of Trans-1, 3, 3, 3-tetrafluoroprop-1-ene and its binary blends, Energy 91 (2015) 386–392.
[8] R. Zhai, Z. Yang, B. Feng, S. Sun, Effect of environmental condition on the flammability limits of two isomers of tetrafluoropropene, Combust. Flame 207 (2019) 295–301.
[9] K. Takizawa, E. Hihara, C. Dang, M. Ito, Risk Assessment of Mildly Flammable Refrigerants, Tech. Rep., Japan Society of Refrigerating and Air Conditioning Engineers, 2017.
[10] V.I. Babushok, G.T. Linteris, Air humidity influence on combustion of R-1234yf (CF_3CFCH_2), R-1234ze(E) (trans-CF_3CHCHF) and R-134a (CH_2FCF_3) refrigerants, Combust. Flame 262 (2024) 113352.
[11] American Society of Heating, Refrigerating and Air-Conditioning Engineers (ASHRAE), Addendum to ANSI/ASHRAE Standard 34-2022: Designation and Safety Classification of Refrigerants, 2022.
[12] R.P. Reed, J.J. Rizzo, Combustibility and Stability Studies of CFC Substitudes with Simulated Motor Failures in Hermetic Refrigeration Equipment, 18th International Congress of Refrigeration (1991).
[13] D.W. Declava, Flammability and reactivity of select HFCs and mixtures, ASHRAE J. 35 (1993) 40–47.
[14] Y.A. Lisochkin, V.I. Poznyak, Explosion hazard of mixtures of poorly combustible chladones with air at elevated pressures, Combust. Explo. Shock. 37 (2001) 27–29.
[15] R.R. Burrell, G.T. Linteris, D.R. Burgess, Jr., M.J. Hegetschweiler, J. Manion, V.I. Babushok, R-152a/air and R-134a/oxygen Constant Volume Spherical Flame Burning Velocity Measurements, 11th US National Meeting of the Combustion Institute (2019).
[16] K. Takizawa, K. Tokuhashi, S. Kondo, Flammability assessment of CH_2=$CFCF_3$: Comparison with fluoroalkenes and fluoroalkanes, J. Hazard. Mater. 172 (2009) 1329–1338.
[17] R.R. Burrell, J.L. Pagliaro, G.T. Linteris, Effects of stretch and thermal radiation on difluoromethane/air burning velocity measurements in constant volume spherically expanding flames, Proc. Combust. Inst. 37 (2019) 4231–4238.
[18] J.L. Pagliaro, G.T. Linteris, P.B. Sunderland, P.T. Baker, Combustion inhibition and enhancement of premixed methane–air flames by halon replacements, Combust. Flame 162 (2015) 41–49.
[19] J.L. Pagliaro, G.T. Linteris, V.I. Babushok, Premixed flame inhibition by $C_2HF_3Cl_2$ and C_2HF_5, Combust. Flame 163 (2016) 54–65.
[20] K. Takizawa, A. Takahashi, K. Tokuhashi, S. Kondo, A. Sekiya, Reaction stoichiometry for combustion of fluoroethane blends, ASHRAE Tran. 112 Part 2 (2006) 459–468.
[21] M.J. Hegetschweiler, G.T. Linteris, Data Reduction Tool for Spherical Constant Volume Flame Experiments, NIST Tech. N., 2021.
[22] M. Elia, M. Ulinski, M. Metghalchi, Laminar burning velocity of methane–air–diluent mixtures, J. Eng. Gas Turb. Power 123 (2000) 190–196.
[23] M.J. Hegetschweiler, L. Berger, R. Hesse, J. Beeckmann, C. Bariki, H. Pitsch, G.T. Linteris, Data reduction considerations for the burning velocity of spherical constant volume flames of R32 (CH_2F_2) with air, Combust. Flame 254 (2023) 112807.
[24] Z. Chen, Effects of radiation and compression on propagating spherical flames of methane/air mixtures near the lean flammability limit, Combust. Flame 157 (2010) 2267–2276.
[25] B.N. Taylor, C.E. Kuyatt, Guidelines for Evaluating and Expressing the Uncertainty of NIST Measurement Results, NIST Tech. N., 1993.
[26] Z. Chen, M.P. Burke, Y. Ju, Effects of compression and stretch on the determination of laminar flame speeds using propagating spherical flames, Combust. Theor. Model. 13 (2009) 343–364.
[27] A. Moghaddas, C. Bennett, E. Rokni, H. Metghalchi, Laminar burning speeds and flame structures of mixtures of difluoromethane (HFC-32) and 1,1-difluoroethane (HFC-152a) with air at elevated temperatures and pressures, HVAC R. Res. 20 (2014) 42–50.
[28] C. Bariki, C. Schwenzer, R. Hesse, R. Glaznev, H. Pitsch, J. Beeckmann, A well-defined methodology to extract laminar flame speeds at engine-relevant conditions, Combust. Flame 268 (2024) 113612.
[29] H. Pitsch, R. Langer, FlameMaster: A C++ computer program for 0D combustion and 1D laminar flame calculations, 2023, Version 4.4.0.
[30] D.G. Goodwin, H.K. Moffat, I. Schoegl, R.L. Speth, B.W. Weber, Cantera: An Object-oriented Software Toolkit for Chemical Kinetics, Thermodynamics, and Transport Processes, Zenodo, 2024.
[31] D.R. Burgess, Jr., Xsenkplot. National Institute of Standards and Technology, Gaithersburg, MD.
[32] D.R. Burgess, Jr., M.R. Zachariah, W. Tsang, P.R. Westmoreland, Thermochemical and chemical kinetic data for fluorinated hydrocarbons, Prog. Energ. Combust. 21 (1995) 453–529.
[33] V.I. Babushok, G.T. Linteris, O.C. Meier, Combustion properties of halogenated fire suppressants, Combust. Flame 159 (2012) 3569–3575.
[34] G.T. Linteris, D.R. Burgess, Jr., F. Takahashi, V.R. Katta, H.K. Chelliah, O. Meier, Stirred reactor calculations to understand unwanted combustion enhancement by potential halon replacements, Combust. Flame 159 (2012) 1016–1025.

[35] J. Santner, F.M. Haas, Y. Ju, F.L. Dryer, Uncertainties in interpretation of high pressure spherical flame propagation rates due to thermal radiation, Combust. Flame 161 (2014) 147–153.
[36] Z. Chen, On the accuracy of laminar flame speeds measured from outwardly propagating spherical flames: Methane/air at normal temperature and pressure, Combust. Flame 162 (2015) 2442–2453.
[37] C. Xiouris, T. Ye, J. Jayachandran, F.N. Egolfopoulos, Laminar flame speeds under engine-relevant conditions: Uncertainty quantification and minimization in spherically expanding flame experiments, Combust. Flame 163 (2016) 270–283.
[38] J.K. Tavares, V. Gururajan, J. Jayachandran, Effects of radiation heat loss on planar and spherical hydrofluorocarbon/air flames, Combust. Flame 258 (2023) 113067.
[39] R. Hesse, C. Bariki, M.J. Hegetschweiler, G.T. Linteris, H. Pitsch, J. Beeckmann, Elucidating the challenges in extracting ultra-slow flame speeds in a closed vessel – A CH_2F_2 microgravity case study using optical and pressure-rise data, Proc. Combust. Inst. 39 (2022) 1783–1792.
[40] R. Glaznev, C. Schwenzer, R. Hesse, S. Girhe, F. Halter, C. Chauveau, H. Pitsch, J. Beeckmann, Ultra-slow ammonia flame speeds — A microgravity study on radiation, Proc. Combust. Inst. 40 (2024) 105334.
[41] D.K. Kim, V.I. Babushok, M.J. Hegetschweiler, G.T. Linteris, Flame propagation in blends of R-152a, R-134a, and R-1234yf with air, Combust. Sci. Technol. 196 (2024) 5107–5127.
[42] R. Hesse, R. Glaznev, R. Langer, C. Schwenzer, V. Babushok, G. Linteris, H. Pitsch, J. Beeckmann, Exploring nonlinear flame speed inhibition effects in mixtures of R1234yf and R32 under microgravity conditions, Proc. Combust. Inst. 40 (2024) 105418.
[43] G.T. Linteris, V.I. Babushok, J.L. Pagliaro, D.R. Burgess, Jr., J.A. Manion, F. Takahashi, V.R. Katta, P.T. Baker, Understanding overpressure in the FAA aerosol can test by $C_3H_2F_3Br$ (2-BTP), Combust. Flame 167 (2016) 452–462.
[44] V.I. Babushok, G.T. Linteris, P.T. Baker, Influence of water vapor on hydrocarbon combustion in the presence of hydrofluorocarbon agents, Combust. Flame 162 (2015) 2307–2310.